Cellular/Molecular

CASK Regulates SAP97 Conformation and Its Interactions with AMPA and NMDA Receptors

Eric I. Lin,[1,2]* Okunola Jeyifous,[1,2]* and William N. Green[1,2]

[1]Department of Neurobiology, University of Chicago, Chicago IL 60637 and [2]Marine Biological Laboratory, Woods Hole, Massachusetts 02543

SAP97 interacts with AMPA receptors (AMPARs) and NMDA receptors (NMDARs) during sorting and trafficking to synapses. Here we addressed how SAP97 distinguishes between AMPARs and NMDARs and what role the adaptor/scaffold protein, CASK, plays in the process. Using intramolecular SAP97 Förster resonance energy transfer sensors, we demonstrated that SAP97 is in "extended" or "compact" conformations *in vivo*. SAP97 conformation was regulated by a direct interaction between SAP97 and CASK through L27 protein-interaction domains on each protein. Unbound SAP97 was mostly in the compact conformation, while CASK binding stabilized it in an extended conformation. In HEK cells and rat hippocampal neurons, SAP97 in the compact conformation preferentially associated and colocalized with GluA1-containing AMPARs, and in the extended conformation colocalized with GluN2B-containing NMDARs. Altogether, our findings suggest a molecular mechanism by which CASK binding regulates SAP97 conformation and its subsequent sorting and synaptic targeting of AMPARs and NMDARs during trafficking to synapses.

Introduction

AMPA receptor (AMPAR) and NMDA receptor (NMDAR) trafficking at postsynaptic densities (PSDs) is critical for the development, function, and plasticity of excitatory synapses. SAP97 is a member of the family of PSD-95-like membrane-associated guanylate kinases (PSD-MAGUKs). PSD-MAGUKs are scaffold proteins that regulate AMPAR and NMDAR trafficking and numbers at PSDs (Elias and Nicoll, 2007; Xu, 2011). The major isoform of SAP97, SAP97β, contains an N-terminal L27 domain, which interacts with other L27 domain-containing proteins, in particular, CASK (Lee et al., 2002). Small numbers of a different SAP97 isoform with an alternative N-terminal domain, SAP97α, also exist in neurons (Waites et al., 2009). In this study, we only assay the SAP97β isoform, referred to as "SAP97" throughout.

SAP97 directly associates with AMPARs and NMDARs early in the secretory pathway (Sans et al., 2001; Jeyifous et al., 2009) via the GluA1 and GluN2A/B PDZ-binding motifs and SAP97 PDZ domains 1 and 2 (Leonard et al., 1998). AMPARs and NMDARs are sorted from each other at the endoplasmic reticulum (Jeyifous et al., 2009) and trafficked from soma to synapses in distinct complexes. SAP97 trafficks with AMPARs and NMDARs on vesicles that move along dendritic microtubules (Setou et al., 2000, 2002) at different rates (Washbourne et al., 2002; Perestenko and Henley, 2003). In addition to SAP97, AMPAR and NMDAR complexes contain different adapters and motors (Setou et al., 2002). Previously, we found that SAP97-CASK interactions are critical for sorting NMDARs from AMPARs, that SAP97 and CASK colocalize in complexes with NMDARs in KIF17-containing transport vesicles in dendrites, and that SAP97, but not CASK, is critical for AMPAR trafficking (Jeyifous et al., 2009). Here, we address how SAP97 distinguishes between the receptor subtypes and the differential role of CASK.

An unexplored possibility is that SAP97 conformational changes regulate their associations with glutamate receptor subtypes. There is significant evidence of different SAP97 conformations *in vitro*. Intramolecular interactions between PSD-MAGUK SH3 and GUK domains regulate GUK affinity for its ligands (McGee et al., 2001; Tavares et al., 2001). Molecular modeling suggests that SAP97 domains are stable in multiple conformational states (Wu et al., 2000) and single particle electron microscopy (EM) revealed SAP97 in both "extended" rod-like and "compact" C-shaped structures (Nakagawa et al., 2004). Using dynamic measurements *in vitro*, a truncated version of SAP97 was found in both compact and extended conformations, in dynamic equilibrium between the two states (Tully et al., 2012). Together, the data raise the possibility that SAP97 function is regulated by conformational changes *in vivo*.

To detect changes in SAP97 conformation *in vivo*, we generated Förster resonance energy transfer (FRET) biosensors by fusing a pair of FRET probes to the N and C termini of SAP97. Using this FRET sensor, we show that SAP97 is in different conformations when bound to AMPARs or NMDARs in HEK cells or in transport vesicles in neurons. SAP97 was in the compact confor-

Received Feb. 21, 2013; revised June 9, 2013; accepted June 14, 2013.

Author contributions: E.I.L., O.J., and W.N.G. designed research; E.I.L. and O.J. performed research; E.I.L. and O.J. analyzed data; E.I.L., O.J., and W.N.G. wrote the paper.

This work was supported by the U.S. National Institutes of Health (NIH) under grant numbers NS043782, MH081251, and DA019695 (W.N.G.). This project was also supported by the National Center for Research Resources and the National Center for Advancing Translational Sciences of the National Institutes of Health through Grant Number UL1 RR024999 (O.J.) and faculty fellowships from the Marine Biological Laboratory. We are grateful to Drs. Anitha Govind, Sarah Antinone, Jason Schumer (University of Chicago), and Xiaobing Chen and Tom Reese (NIH/National Institute of Neurological Disorders and Stroke) for their critical reading and helpful comments on this manuscript. We thank Vytas Bindokas and Paul Selvin for their technical support with FRET experiments and Shohei Koide for his assistance in generating the SAP97 L27 mutant.

The authors declare no competing financial interests.

*E.I.L. and O.J. contributed equally to this work.

Correspondence should be addressed to William N. Green, Department of Neurobiology, University of Chicago, Chicago IL 60637. E-mail: wgreen@bsd.uchicago.edu.

DOI:10.1523/JNEUROSCI.0816-13.2013

Copyright © 2013 the authors 0270-6474/13/3312067-10$15.00/0

mation when colocalized with GluA1-containing AMPARs, and in the extended conformation when colocalized with GluN2B-containing NMDARs. An interaction between SAP97 and CASK changes SAP97 conformation from compact to extended. Our findings explain why CASK selectively colocalized with NMDARs and SAP97 in transport vesicles, and why knockdown of SAP97 impaired trafficking of AMPARs and NMDARs but CASK knockdown only affected NMDAR trafficking (Jeyifous et al., 2009). Overall, our results provide new insights into how changes in SAP97 conformation regulate their function and reveal how CASK binding alters SAP97 conformation and controls its interactions with AMPARs and NMDARs.

Materials and Methods

Culture of HEK293 cells and primary hippocampal neurons

HEK293 cells were maintained in DMEM supplemented with 10% calf serum (HyClone). Cells were transiently transfected with cDNA using a calcium phosphate protocol (Claudio, 1992). Cells transfected with HA-GluR1 or HA-NMDAR were maintained in media containing 1 mM kynurenic acid (Sigma) or 100 μM D(−)-2-amino-5-phosphonovaleric acid (Sigma) and 10 μM MK-801 (RBI), respectively, to prevent excitotoxicity.

Hippocampal cultures were prepared using Neurobasal medium, 2% (v/v) B27, and 2 mM L-glutamine. Briefly, hippocampi from embryonic (E18–E19) Sprague Dawley rats of either sex were dissected, dissociated in 0.05% trypsin (v/v; Invitrogen), and cells were plated at a density of $\sim 4 \times 10^5$ cells/ml on polyethylenimine-coated 12 mm coverslips. Coverslips were maintained in Neurobasal medium containing B27 and GlutaMAX (all from Invitrogen).

Neuronal cultures were transfected at 12–14 days *in vitro* (DIV) with the Lipofectamine 2000 transfection reagent (Invitrogen) according to manufacturer's recommendations, with the exception that 1–2.5 μg of each cDNA in 62.5 μl of Neurobasal media and 2.5 μl of Lipofectamine 2000 in 62.5 μl of Neurobasal media were mixed and added to coverslips in 12-well plates.

Antibodies and reagents. The following antibodies were used: anti-Bassoon antibody (Synaptic Systems), anti-NR2B antibody (BD Biosciences), anti-GluR1 antibody (Calbiochem), anti-HA (rabbit polyclonal) antibody (Bethyl Laboratories), anti-Myc 9E10 antibody (Santa Cruz Biotechnology), anti-GFP antibody (Sigma-Aldrich), and anti-RFP antibody (MBL International). Alexa Fluor anti-mouse 488/568/647/750 and Alexa Fluor anti-rabbit 647/750 were purchased from Invitrogen.

Plasmids and transfections. Rat GluN1 and GluN2B were obtained from J. Boulter (University of California, Los Angeles). GluN1 and GluN2B subunits were tagged at the NH_2 terminus with the FLAG (DYKDDDDK) and HA (YPYDVPDYA) epitopes respectively using the extension overlap PCR method (Ho et al., 1989) and subcloned into a pCB6 mammalian expression vector. Monomeric cherry (Ch)-tagged GluA1 was a gift from C. Garner (Stanford University, Stanford, California). Myc-CASK and Myc-CASKΔL27N were gifts from B. Margolis (University of Michigan). Construction of GFP-SAP97β (splice variant I1b, I3, and I5) has been previously described (Wu et al., 1998; Bresler et al., 2004). To generate Ch-SAP97-V, Ch-SAP97, and SAP97-V, EcoRI restriction enzyme sites were placed on the N and C termini of mCherry and KpnI sites were placed on the N and C termini of Venus using PCR. Using *EcoR1* and KpnI, mCherry and/or Venus were subcloned into SAP97β in pEGFP-N1 and screened for correct directional insertion. To generate Ch-SAP97-V-L15K, amino acid residue 15 was mutated from UUG to AAG using QuikChange (Invitrogen).

Immunostaining and image analysis. HEK293 cells and neuronal cultures (24 h post-transfection) were washed twice in PBS at 22–25°C, fixed in 4% paraformaldehyde (PFA)/sucrose (v/v, room temperature, 10 min), and washed three times in PBS (5–10 min). For permeabilization, cells were incubated in 0.1% Triton-X in PBS (10 min), incubated in blocking solution (2% glycine (w/v), 2% bovine serum albumen (w/v), 0.2% gelatin (w/v), and 50 mM NH_4Cl in PBS; 10 min) and then incubated with the indicated primary antibody diluted in blocking solution (1 h). Following primary antibody incubation, cells were washed three times in blocking solution (5–10 min) and overlaid with an appropriate secondary antibody diluted in blocking solution (1 h). Cells were then washed three times in PBS (5–10 min) and the slips mounted in 80% glycerol or Prolong Gold (Invitrogen). Fluorescence images were acquired using a Leica SP5 Tandem Scanner Spectral 2-photon scanning confocal microscope (Leica Microsystems). Images were processed using ImageJ (National Institutes of Health, Bethesda, MD) and Adobe Photoshop software.

Calculation of FRET efficiency. Images were acquired using a Leica SP5 laser scanning confocal microscope operating with an argon laser tuned to 514 nm, a DPSS laser tuned to 561 nm, and an HeNe laser line tuned to 633 nm. Cells were examined with a 63× 1.4 NA (Leica) oil-immersion objective and 4× zoom. FRET was measured using the acceptor photobleaching method (Kenworthy, 2001). Cells were bleached in the mCherry channel by scanning a region of interest 5–10 times using the 561 nm DPSS laser line at 100% intensity. The time of bleach ranged from 3 to 10 s depending on the size of the region of interest (ROI) for bleaching. For HEK293 cells, a scanning speed of 800 Hz was used to maximize the degree of acceptor bleaching at each step. For neurons, a scanning speed of 8000 Hz was used. Before and after each bleach step, Venus images were collected to assess changes in donor fluorescence. Because increases in Venus fluorescence caused by bleaching of the mCherry acceptor could potentially be masked by bleaching of Venus related simply to the imaging process itself, the effect of photobleaching due to imaging was minimized by collecting Venus images at 1% of the laser intensity. To ensure that bleaching due to imaging was minimal, we monitored the level of bleaching in each experiment by collecting five images of the donor (Venus) before bleaching. The gain of the photomultiplier tubes was adjusted so as to eliminate cross talk and to achieve the best possible dynamic range.

To calculate the FRET energy transfer efficiency (E_T), we used the following formula:

$$E_T = (1 - I_{da}/I_d)$$

where I_{da} and I_d are the fluorescence intensities of the donor in the presence and absence of acceptor, respectively. To obtain these values, fluorescence intensities were analyzed using ImageJ software and donor fluorescence variations were plotted against acceptor depletion over successive bleaching steps. The slope of the linear relationship was used to I_{da} and I_d. As a reference, fluorescence of analogous peptides with only a donor, only an acceptor, or both were measured to control for both pseudo-FRET artifacts and intermolecular FRET. Average distance (r) between donor and acceptor was calculated using the following formula:

$$r = R_0(E_T^{-1} - 1)^{1/6}$$

where R_0 is the Förster distance corresponding to 57 Å for our Venus and mCherry sensors. This calculation assumes a random orientation factor ($\kappa^2 = 2/3$).

To prepare HEK293 cells for FRET analysis, cells were fixed in 4% PFA/sucrose, washed in PBS, and mounted in 80% glycerol. To define ROIs with cell markers (i.e., AMPARs, NMDARs, presynaptic markers, etc.), immunolabeling was performed with primary antibody, washed three times, and labeled with an Alexa 647- or Alexa 750-conjugated secondary antibody, which was imaged on the Far Red or Far Far Red channel at the end of a photobleaching protocol. Images of these markers were used to create a mask to isolate regions for FRET analysis.

Argon lasers (514 and 568 nm) were used to excite Venus and mCherry, respectively (spectral channel settings: donor, 535 nm ± 10 nm; acceptor 610 nm ± 25 nm). Low resonant scanning at 800 Hz was used in HEK293 cell experiments while high-resonant scanning at 8000 Hz was used for neuron experiments.

Immunoprecipitation and immunoblot analysis. Cells were pelleted by brief centrifugation, resuspended, washed once with PBS, and solubilized in lysis buffer (150 mM NaCl, 5 mM EDTA, pH 7.4, 50 mM Tris, pH 7.4, 0.02% NaN_3) containing 1% Triton X-100 + NEM (2 mM), phenylmethanesulfonyl fluoride (2 mM), leupeptin (10 g ml^{-1}), *N*-tosyl-Lys-chloromethyl ketone HCl (10 g ml^{-1}), chymotrypsin (10 g ml^{-1}), and pepstatin (10 g ml^{-1}). Following a 1 h solubilization (4°C), samples were centrifuged at 14,000 × *g* for 30 min at 4°C. Subsequent analyses were

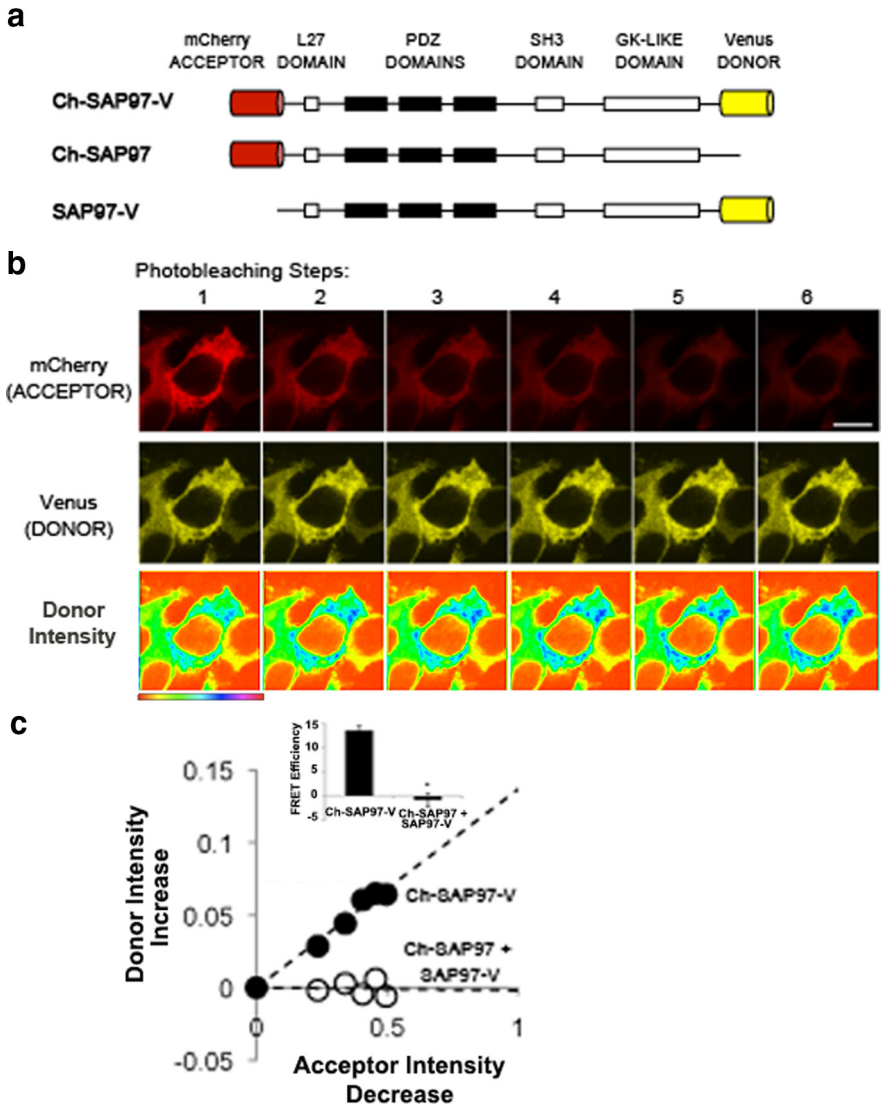

Figure 1. An intramolecular FRET sensor designed to assay SAP97 conformation. ***a***, Schematic of SAP97 FRET sensor, Ch-SAP97-V, and FRET sensor controls, Ch-SAP97 and SAP97-V. ***b***, Representative images of a photobleaching method performed on Ch-SAP97-V in HEK293 cells to obtain Ch-SAP97-V FRET efficiency. Venus and mCherry fluorescence images were acquired before and after six acceptor photobleaching steps. Bottom row displays Venus (donor) pseudocolor intensity. Scale bar, 10 μm. ***c***, Ch-SAP97-V FRET efficiency determined from the linear relationship between increases in donor (mCherry) fluorescence with decreases in acceptor (Venus) with photobleaching. The photobleaching steps for Ch-SAP97-V in ***b*** are plotted as the percentage decrease in acceptor intensity versus the percentage increase in donor intensity (●). A corresponding rise in donor intensity is not observed when Ch-SAP97 is coexpressed with SAP97-V (○). Inset, FRET efficiency values, E_T, were calculated from the data above using the equation: $E_T = (1 - I_{da}/I_d)$, where I_{da} and I_d are the fluorescence intensities of the donor in the presence and absence of acceptor, respectively. FRET efficiency for Ch-SAP97-V is 13.5 ± 1% (mean ± SEM; $n = 34$ cells, $^*p < 0.01$) compared with −0.8 ± 1.8% (mean ± SEM; $n = 15$ cells) in cells coexpressing Ch-SAP97 and SAP97-V.

performed using the Triton X-100-soluble fraction. Immunoprecipitations were performed by overnight antibody incubation at 4°C. Protein-antibody complexes were isolated by incubation with Protein G–Sepharose for 3 h at 4°C.

For immunoblotting, proteins separated by SDS-PAGE were transferred to PVDF membranes. After transfer, the PVDF was blocked with 3% milk in wash buffer (10 mM Tris, pH 7.4, 0.05% Tween 20 (w/v), and 150 mM NaCl). Membranes were washed briefly in wash buffer and then incubated for 1 h with primary antibodies. The blots were washed and incubated with secondary antibody (goat antibody to mouse, rabbit, or chicken Alexa 488, 568, or 647) at the appropriate dilution for 1 h. After washing, membranes were imaged on Bio-Rad Molecular Imager Pharos-FX. Quantification was done using ImageJ.

Statistical analysis

Results are expressed as mean ± SEM of n samples unless stated otherwise. Statistical significance was assessed by a two-tailed Student's t test or ANOVA as appropriate.

Results

Generation of SAP97 FRET sensor to detect conformational changes

SAP97 is required for sorting NMDARs from AMPARs in the endoplasmic reticulum (ER; Jeyifous et al., 2009) and interacts directly with both NMDARs and AMPARs (Sans et al., 2001; Elias and Nicoll, 2007; Jeyifous et al., 2009). Our goal was to understand how SAP97 distinguishes between AMPARs and NMDARs and whether this involves different conformations of SAP97 that have previously been reported (Nakagawa et al., 2004). To assay for changes in SAP97 conformation, we generated SAP97 fusion constructs by adding fluorescent proteins that form a FRET pair to the N and C termini of SAP97 (Ch-SAP97-V; Fig. 1*a*). A mCherry and Venus fluorophore were selected as an acceptor and donor pair. To assay for FRET, we performed an acceptor photobleaching protocol on Ch-SAP97-V (Fig. 1*b*,*c*) from which we obtained FRET efficiency values (Fig. 1*c*, inset). The protocol measured increases in Venus fluorescence (donor; Fig. 1*b*, middle and bottom) after successive photobleaching of mCherry (acceptor; Fig. 1*b*, top). The increase in donor fluorescence, which is best visualized by pseudocolorization of the donor fluorescence (Fig. 1*b*, bottom), is a quantitative measure of FRET based on the blocking of donor fluorescence quenching caused by FRET. The percentage change in donor fluorescence increased linearly as the acceptor fluorescence decreased (Fig. 1*c*). The FRET efficiency, 13.5%, was calculated from the fit to the values of the fluorescence changes. Importantly, no FRET was observed when the FRET pairs were attached separately to the N or C termini of SAP97 (Ch-SAP97 and SAP97-Venus; Fig. 1*a*) and expressed together in HEK293 cells (Fig. 1*c*). The FRET measured using Ch-SAP97-V is, therefore, intramolecular and does not result from intermolecular FRET between two or more SAP97 molecules. These results also indicate that donor photoactivation, which can sometimes occur during acceptor photobleaching, is not contributing to the FRET measurements (Karpova and McNally, 2006). If we assume a random orientation factor for FRET pairs, the FRET efficiency value corresponds to a distance between FRET pairs of ~77Å, which is consistent with previous EM studies of SAP97 in the compact conformation (Nakagawa et al., 2004). Similar values for the FRET efficiency were obtained when a different SAP97 FRET sensor that used Venus and ECFP as a FRET pair (Venus-SAP97-ECFP; data not shown) was assayed.

SAP97 is in different conformations when interacting with AMPARs and NMDARs

In neurons, SAP97 and GluA1 co-cluster in puncta on the cell surface and in an intracellular compartment (Sans et al., 2001). Similar cell surface and intracellular puncta containing Ch-SAP97 and GluA1 subunits are observed when expressed in HEK293 cells (Jeyifous et al., 2009). We observed identical colocalizing cell-surface and intracellular puncta for the FRET sensor, Ch-SAP97-V, with GluA1 subunits in HEK293 cells (Fig. 2*a*). We assayed Ch-SAP97-V FRET when colocalized in small intracellular (Fig. 2*a*, top) or cell-surface clusters (Fig. 2*a*, bottom) with GluA1-containing AMPARs, assuming that Ch-SAP97-V and GluA1 subunits in the clusters are complexed. There was a small difference in Ch-SAP97-V FRET in these clusters compared with Ch-SAP97-V without AMPAR colocalization (Fig. 1), but the difference was not statistically significant. The FRET efficiency for theCh-SAP97-V sensor alone was 13.5% (Fig. 1) and 14.4% when clustered with AMPARs at the cell surface (Fig. 2*a*,*c*).

In HEK293 cells, interactions between SAP97 and GluN2B subunits cause intracellular clusters of SAP97 and NMDARs to form in the ER, which prevent NMDAR trafficking to the cell surface (Jeyifous et al., 2009). We observed the same intracellular clusters when the FRET sensor, Ch-SAP97-V, was coexpressed with NMDAR subunits (Fig. 2*b*). When complexed with NMDARs at these intracellular clusters, the FRET efficiency of Ch-SAP97-V significantly decreased to 2.6% compared with 13.5% when alone (Fig. 2*b*,*c*). The decreased FRET efficiency of SAP97 to near 0% when associated with NMDARs is consistent with a conformation that places its N and C termini at or beyond 100 Å apart in an "extended" conformation as observed by EM single particle measurements (Nakagawa et al., 2004). This result indicates that SAP97 changes from a compact to extended conformation before or during associations with NMDARs. We obtained almost identical results in HEK293 cells with the different SAP97 FRET sensor (Venus-SAP97-ECFP; data not shown).

Next, we expressed Ch-SAP97-V in primary hippocampal cultured neurons (Fig. 2*d*). In the somata, Ch-SAP97-V labeled reticulated membrane, consistent with previous findings of endogenous SAP97 in the ER (Fig. 2*d*, left). In dendrites, we observed Ch-SAP97-V in two classes of puncta that we had previously observed for endogenous and transfected SAP97 (Jeyifous et al., 2009). Large puncta containing Ch-SAP97-V were observed in spine-like structures that colocalized with the presynaptic marker, bassoon (Fig. 2*d*, middle and right), consistent with a postsynaptic localization for Ch-SAP97-V. Smaller, nonsynaptic puncta were also observed in the dendritic shafts (Fig. 2*d*, right). We had previously found that SAP97 in these smaller puncta were mobile vesicles, some of which contained NMDARs (Jeyifous et al., 2009). These smaller puncta in the shafts of dendrites contain AMPARs or NMDARs in separate vesicles (Washbourne et al., 2002) and SAP97 interacts with GluA1-containing AMPARs (Leonard et al., 1998) or GluN2B-containing NMDARs (Jeyifous et al., 2009).

To examine SAP97 conformation in neurons when colocalized with NMDARs or AMPARs, we analyzed the smaller puncta in the shafts of dendrites. Endogenous NMDARs or AMPARs were labeled with anti-GluA1 or anti-GluN2B antibodies, respectively (Fig. 2*e*,*f*). In these cultures, ~20% of immunolabeled GluA1 puncta appeared to be synaptic based on colocalization with the presynaptic marker, bassoon. The other 80% of GluA1-containing puncta were nonsynaptic and we assumed they are mostly transport vesicles. The SAP97 FRET efficiency measured at puncta that colocalized with GluA1 was 27.2%, significantly higher than the 5.2% measured at puncta that did not colocalize with GluA1 (Fig. 2*e*,*g*). We obtained completely opposite FRET results for Ch-SAP97-V puncta that either colocalized or did not colocalize with anti-GluN2B antibodies. For puncta with GluN2B subunits, the SAP97 FRET efficiency was 3.5% compared with 26.2% for puncta that did not colocalize with GluN2B subunits (Fig. 2*f*,*g*). Thus, our findings in neurons are consistent with the results in HEK293 cells and indicate that SAP97 is primarily in the compact conformation when associated with AMPARs in transport vesicles, and in the extended conformation when associated with NMDARs in transport vesicles.

CASK binding to SAP97 triggers a transition to the extended conformation

During normal NMDAR trafficking in cultured hippocampal neurons, NMDARs are bound by SAP97 through a PDZ domain interaction, and SAP97 is bound by CASK through L27 domains on each protein (Lee et al., 2002; Jeyifous et al., 2009). AMPAR trafficking also requires a PDZ domain interaction with SAP97 (Sans et al., 2001), but does not appear to be bound by CASK (Jeyifous et al., 2009). These findings prompted us to study whether CASK binding to SAP97 could be a determinant in altering SAP97 conformation and regulating whether it interacts with AMPARs or NMDARs. We coexpressed Ch-SAP97-V and Myc-tagged CASK (Myc-CASK; Fig. 3*a*) in HEK293 cells (Fig. 3*b*, third row) and measured SAP97 FRET at the cell surface where it colocalizes with CASK. CASK significantly decreased Ch-SAP97-V FRET efficiency to 2.6% (Fig. 3*c*) compared with 13.5% when Ch-SAP97-V was expressed alone (Fig. 3*b*, top row). A similar decrease caused by CASK was also observed using a different Venus-SAP97-ECFP FRET sensor (data not shown). In both cases, the loss of FRET to near 0% indicates that coexpression with CASK causes SAP97 to change its predominant conformation from the compact to the extended form.

Next, we examined whether the decrease in Ch-SAP97-V FRET with CASK coexpression occurred through a direct interaction between CASK and SAP97. Previous studies concluded that the SAP97-CASK interaction is an L27 domain association between the L27 domain at the N terminus of SAP97 and the first of two L27 domains (L27N) on CASK (Lee et al., 2002). We tested whether a CASK construct in which the first of its two L27 domains was truncated (Myc-CASKΔL27N; Fig. 3*a*) prevented the SAP97-CASK interaction. When we coexpressed Myc-CASKΔL27N with Ch-SAP97-V in HEK293 cells we did not observe colocalization between SAP97 and CASKΔL27N at the plasma membrane, which we observed when Ch-SAP97-V was coexpressed with full-length CASK (Fig. 3*b*). We also could not coimmunoprecipitate Ch-SAP97-V with Myc-CASKΔL27N while Ch-SAP97-V coimmunoprecipitated with full-length CASK (Fig. 3*d*). As a second test of the SAP97-CASK interaction, we introduced a more subtle change in the Ch-SAP97-V L27 domain to disrupt the L27 domain interaction. Based on the high-resolution NMR structure of the interacting SAP97 and CASK L27 domains (Feng et al., 2004), we predicted that a leucine residue (L15) in a hydrophobic binding surface of the SAP97 L27 domain, when mutated to a lysine residue (L15K-Ch-SAP97-V), would disrupt the L27 interaction between SAP97 and CASK. Similar to the Myc-CASKΔL27N truncation, the L15K-Ch-SAP97-V mutation did not colocalize with CASK in HEK293 cells (Fig. 3*b*) nor did it coimmunoprecipitate with CASK (Fig. 3*d*).

When Ch-SAP97-V was coexpressed with CASKΔL27N instead of CASK, the decrease in Ch-SAP97-V FRET was no longer observed, consistent with the FRET decrease being caused by an

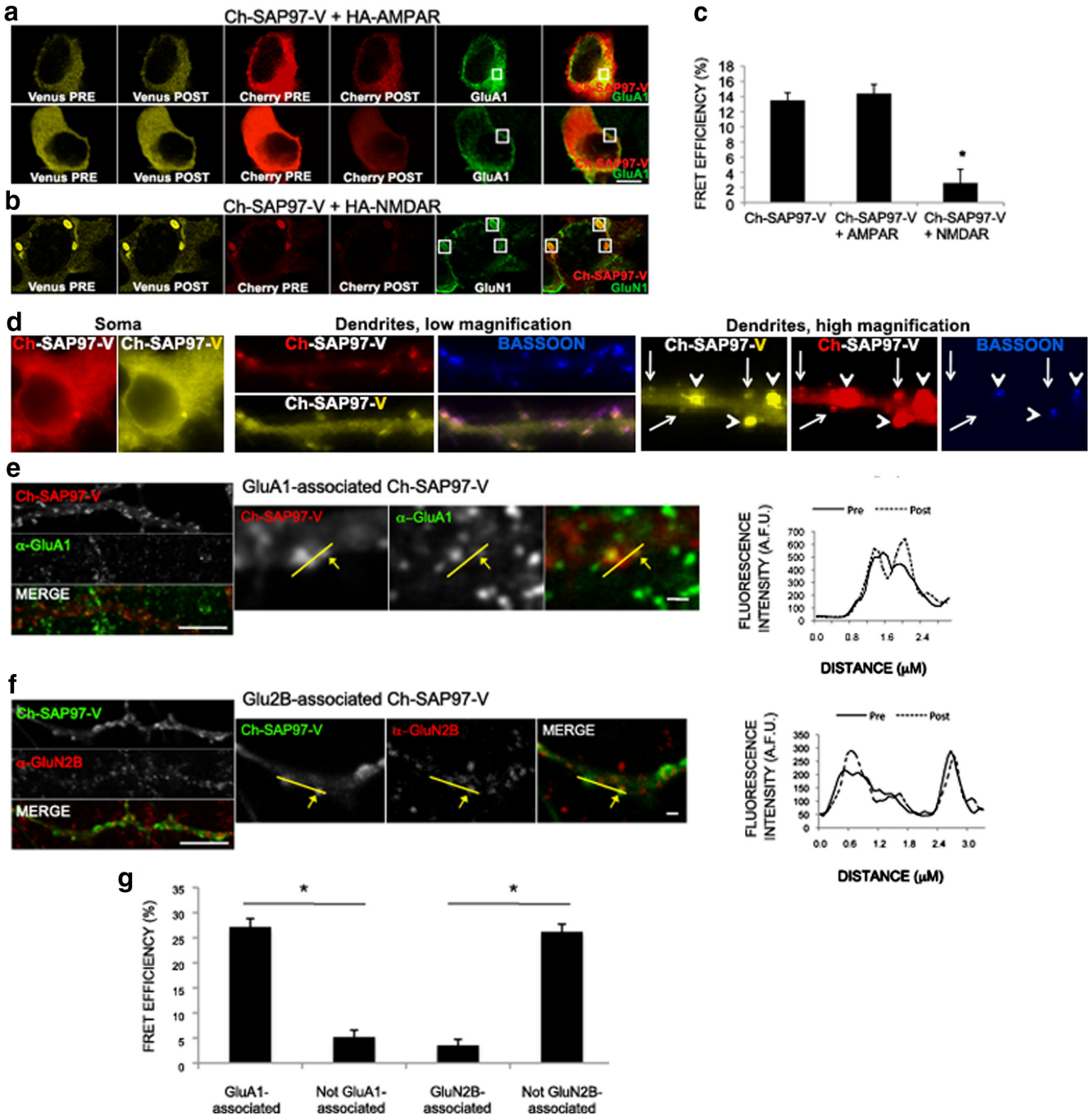

Figure 2. SAP97 is in different conformations when associated with NMDARs and AMPARs. ***a***, Images from HEK293 cells coexpressing Ch-SAP97-V and HA-tagged AMPARs (HA-GluA1). Intracellular (boxed region, top) and cell-surface (boxed region, bottom) clusters of SAP97 and AMPARs were assayed. Cell-surface clusters of HA-GluA1-containing AMPARs were labeled by staining intact cells to the extracellular HA-GluA1 epitope with anti-HA antibodies. Regions of apparent AMPAR-SAP97 interactions were identified by colocalization of SAP97 fluorescence with staining for HA-tagged GluA1 subunits with anti-HA antibodies (green). The initial and final (pre- and post-bleached) Venus and mCherry fluorescence signals are displayed for Ch-SAP97-V during an acceptor photobleaching experiment. Scale bar, 10 μm. ***b***, Images from HEK293 cells coexpressing Ch-SAP97-V and HA- and Flag-tagged NMDARs (HA-GluN2B and Flag-GluN1). Intracellular clusters of SAP97 and NMDARs (boxed regions) were assayed and identified by colocalization of SAP97 fluorescence with staining for Flag-tagged GluN1 subunits with anti-Flag antibodies (green). The initial and final (pre- and post-bleached) Venus and mCherry fluorescence signals are displayed for Ch-SAP97-V during an acceptor photobleaching experiment. Scale bar, 10 μm. ***c***, Ch-SAP97-V FRET efficiency values at NMDAR or AMPAR clusters. The FRET efficiency of Ch-SAP97-V in AMPAR clusters was 14.4 $\pm$ 1.2% (mean $\pm$ SEM; $n = 18$ cells) and 2.6 $\pm$ 1.8% (mean $\pm$ SEM; $n = 20$ cells, $^*p < 0.01$) in NMDAR clusters. Only the FRET efficiency values for Ch-SAP97-V in NMDAR clusters was significantly different from the FRET efficiency value of 13.5 $\pm$ 0.8% for Ch-SAP97-V expressed alone in HEK293 cells. ***d***, Dual fluor tagging of SAP97 does not disrupt normal neuronal targeting and localization of the protein. Hippocampal neurons (16 DIV) transfected with cDNA encoding Ch-SAP97-V. Left, Somatic expression of the FRET sensor. The perinuclear and ER-like localization is identical to that reported for endogenous SAP97. Middle, Ch-SAP97-V is observed throughout dendritic shafts, with an obvious accumulation in postsynaptic spines (colocalization with the presynaptic protein, Bassoon), as reported for SAP97 β. Right, Higher magnification images displaying Ch-SAP97-V in large, synaptic (arrowheads) puncta, and also in small, nonsynaptic (arrows) puncta that may represent trafficking vesicles. ***e***, The FRET efficiency of Ch-SAP97-V colocalized with AMPARs in dendrites. Left, Images of dendrites from cultured hippocampal neurons (E18, 14 DIV) transfected with Ch-SAP97-V and immunolabeled with anti-GluA1 antibodies to detect endogenous GluA1 colocalized with Ch-SAP97-V (Ch-SAP97-V fluorescence, top; anti-GluA1, middle; merged image, bottom). Scale bar, 10 μm. Middle, Expanded images of Ch-SAP97-V puncta that colocalize with GluA1 (arrow) or do not colocalize. Right, An example of analysis of the donor fluorescence intensity profiles taken through the yellow line in the middle images. Intensity profiles were acquired before (pre; solid line) and after (post; dashed line) acceptor photobleaching. FRET changes were only observed for Ch-SAP97-V puncta colocalized with GluA1. Scale bar, (*Figure legend continues.*)

L27-L27 domain interaction between CASK and SAP97. Similarly, the decrease in Ch-SAP97-V FRET caused by CASK was in large part not observed when L15K-Ch-SAP97-V replaced Ch-SAP97-V. We did observe a small decrease in L15K-Ch-SAP97-V FRET by CASK suggesting that the interaction between L15K-Ch-SAP97-V and CASK was not totally eliminated by the SAP97 mutation. These results suggest that the interaction between the L27N domain of CASK and the L27 domain of SAP97 triggers SAP97 to change its conformation from the compact to the extended conformation. Based on these results, we predicted that the addition of CASK to HEK cells expressing SAP97 and GluA1-containing AMPARs should have a significant effect on SAP97-AMPAR interactions. Specifically, we predicted that the addition of CASK should highly reduce the coimmunoprecipitation of GluA1 subunits with SAP97, if SAP97 conformation changes largely from the compact to extended conformation. Consistent with the prediction, we found in HEK cells that CASK coexpression reduced the coimmunoprecipitation of GluA1 subunits with SAP97 by 84% compared with coimmunoprecipitation of GluA1 subunits and SAP97 in the absence of CASK (Fig. 3*e*).

Other post-translational modifications alter SAP97 conformation

In experiments where SAP97 was expressed in HEK293 cells, the FRET measurements were largely consistent with FRET measurements in neurons. However, we found unexpected differences in the peak FRET value measured for the compact conformations of SAP97 in HEK293 cells compared with cultured neurons (Fig. 3*f*, left). Because of the precision of our FRET measurements, we felt it unlikely that the differences in FRET measurements between neurons and HEK293 cells were an artifact. Rather, there appears to be a difference in the SAP97 compact conformation when expressed in HEK293 cells versus neurons. Therefore we tested whether additional post-translational modifications could account for the difference observed between the two cell types using the SAP97 FRET sensor.

CaMKII phosphorylates the L27 domain (residue S39) and PDZ1 domain (residue S232) of SAP97, which inhibits its interactions with GluN2A (Gardoni et al., 2003; Mauceri et al., 2007). AKAP, GKAP, and L27 proteins such as MyoVI are also known to interact with SAP97 and regulate AMPAR trafficking (Nash et al., 2010; Colledge et al., 2000). To address whether CaMKII activity could influence Ch-SAP97-V conformational state, we compared the FRET efficiency when Ch-SAP97-V was coexpressed with autophosphorylation-deficient CaMKII-T286A, which decreases CaMKII activity, or phosphomimetic CaMKII-T286D, which causes CaMKII to be more active (Fig. 3*f*, right). In HEK293 cells, CaMKII-T286A significantly lowered the FRET efficiency of Ch-SAP97-V while CaMKII-T286D significantly increased FRET efficiency. These results suggest that phosphorylation of SAP97 by CaMKII might contribute to the alteration of SAP97 conformation *in vivo*, but in a more subtle way than the binding and unbinding of CASK, perhaps by modulating the position of the N and C termini relative to each other when in the compact conformation. Because the FRET efficiency values are so low when Ch-SAP97-V is in the extended conformation, we are unlikely to measure these differences. The finding that CaMKII phosphorylation of SAP97 weakens its interaction with NMDARs (Gardoni et al., 2003) suggests that CaMKII phosphorylation of SAP97 when bound by CASK may also modulate SAP97 conformation when it is in the extended conformation.

Discussion

SAP97 and CASK are required for the sorting of AMPARs and NMDARs during their trafficking in dendrites (Jeyifous et al., 2009), but the mechanistic details about how they differentially interact with the receptor subtypes are poorly characterized. In this study, we have tested whether changes in SAP97 conformation have a role in the ability of SAP97 to discriminate between AMPARs and NMDARs. To assay for SAP97 conformation, we engineered an intramolecular SAP97 FRET sensor that allowed us to measure and distinguish SAP97 extended and compact conformations *in vivo*. Previous evidence that SAP97 undergoes dynamic changes between compact and extended conformations *in vitro* comes from a small-angle, x-ray scattering study on a truncated version of SAP97 (Tully et al., 2012). In the present study, we demonstrate that SAP97 exists in extended and compact conformations *in vivo*, and that it is in the extended conformation when NMDAR bound, and in the compact conformation when AMPAR bound. Previously, we had observed that knockdown of either SAP97 or CASK altered the sorting of NMDARs from AMPARs, but knockdown of SAP97, and not CASK, altered AMPAR trafficking (Jeyifous et al., 2009). Consistent with these data, we find that the L27 domain-mediated interaction between SAP97 and CASK stabilizes SAP97 in the extended conformation, the conformation in which it preferentially interacts with NMDARs. The levels of CASK and the degree to which it is bound to SAP97 appear to regulate whether SAP97 binds to NMDARs or AMPARs. In addition to CASK binding, SAP97 conformation was modulated by altering the levels of CaMKII activity. Thus, there appear to be multiple methods by which SAP97 conformation is regulated, and thereby, whether it binds to NMDARs, AMPARs, or other binding partners.

In Figure 4, we propose a model to explain how dynamic conformational changes of SAP97 *in vivo* mediate the sorting and synapse-specific targeting of AMPARs and NMDARs during their trafficking in dendrites. As shown in Figure 4*a*, we assume that SAP97 is in dynamic equilibrium between its compact and extended states *in vivo*. When not bound by CASK, it resides primarily in its compact state and can interact with GluA1-containing AMPARs, but not appreciably with GluN2B-containing NMDARs in the ER. When the SAP97 N terminal, L27 domain binds CASK at its L27N domain, it stabilizes it in its extended conformation. In this state, it can interact with GluN2B-containing NMDARs, forming a CASK-SAP97-NMDAR complex, and does not appreciably interact with GluA1-containing AMPARs. Thus, CASK levels and the degree to which CASK is bound to SAP97 can explain how SAP97 differentially targets AMPARs and NMDARs at the ER (Fig. 4*b*). The

←

(*Figure legend continued.*) 1 μm. ***f***, The FRET efficiency of Ch-SAP97-V colocalized with NMDARs in neurons. Left, Images of dendrites from cultured hippocampal neurons (E18, 14 DIV) transfected with Ch-SAP97-V and immunolabeled with anti-GluN2B antibodies to detect endogenous GluN2B colocalized with Ch-SAP97-V (Ch-SAP97-V fluorescence, top; anti-GluN2B, middle; merged image, bottom). Scale bar, 10 μm. Middle, Expanded images of Ch-SAP97-V puncta that colocalize with GluN2B (arrow) or do not colocalize. Right, An example of analysis of the donor fluorescence intensity profiles taken through the yellow line in the middle images. Intensity profiles were acquired before (pre; solid line) and after (post; dashed line) acceptor photobleaching. FRET changes were only observed for Ch-SAP97-V puncta not colocalized with GluN2B. Scale bar, 1 μm. ***g***, Ch-SAP97-V FRET efficiency values at AMPAR-or NMDAR-containing puncta in dendrites. The FRET efficiency of Ch-SAP97-V in GluA1-associated puncta was 27.2 ± 1.6% and 5.2 ± 1.4% for Ch-SAP97-V in puncta not associated with GluA1 (mean ± SEM; $n = 53$ puncta, 8 cells, $^*p < 0.01$). Ch-SAP97-V FRET efficiency was 3.5 ± 1.2% for puncta associated with GluN2B subunits and 26.2 ± 1.5% for puncta not associated with GluN2B (mean ± SEM; $n = 78$ puncta, 10 cells, $^*p < 0.01$).

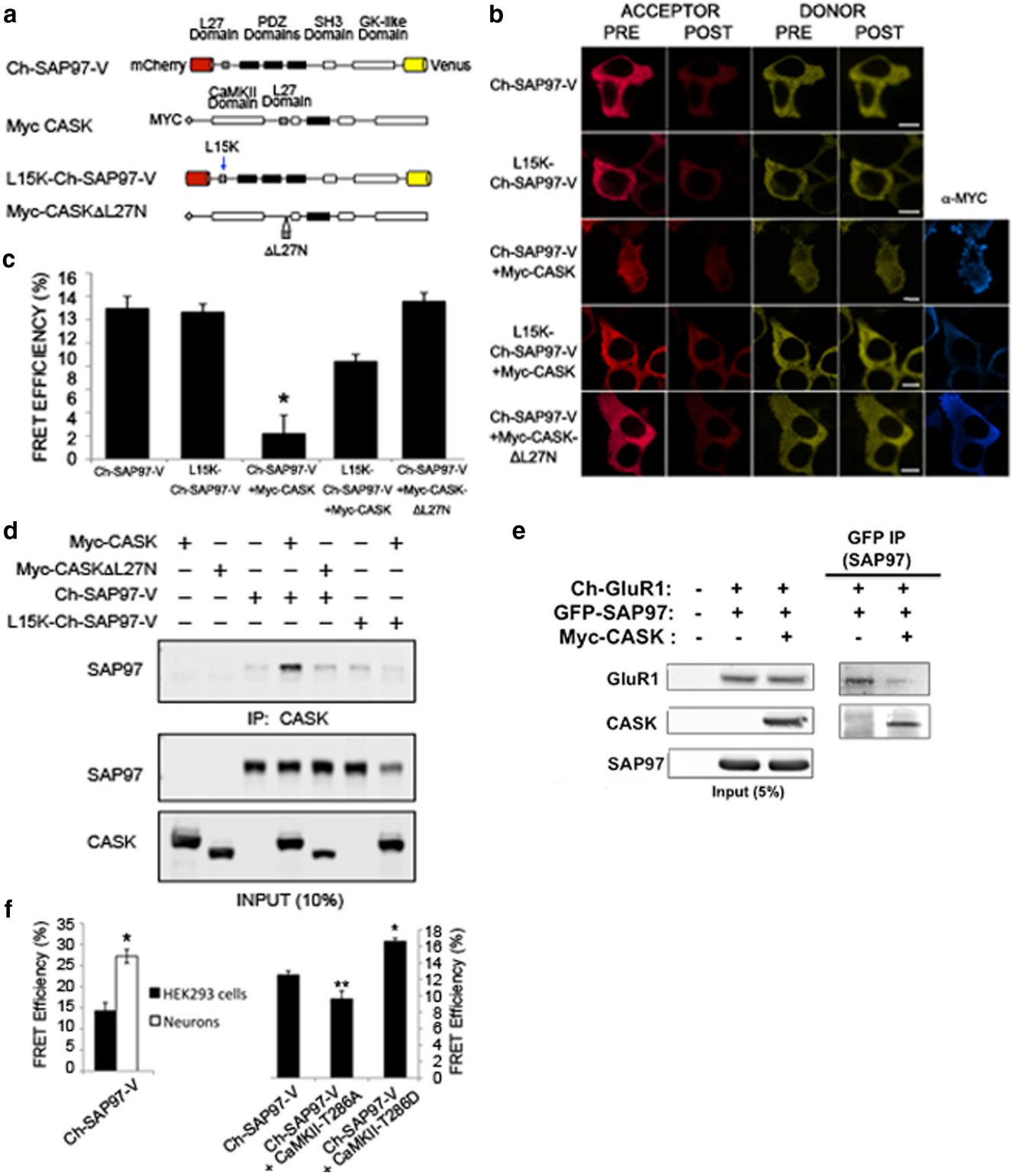

Figure 3. CASK binding to SAP97 triggers a change in SAP97 conformation. ***a***, Schematic of SAP97 and CASK L27 domain mutation constructs, L15K-Ch-SAP97-V and Myc-CASK-ΔL27N. ***b***, Representative images of FRET analysis in HEK293 cells expressing the indicated Ch-SAP97-V and Myc-CASK constructs. Images of Ch-SAP97-V fluorescence are the initial and final (pre and post) Venus and mCherry fluorescence signals acquired over the course of acceptor photobleaching. Myc-CASK was detected with anti-Myc antibodies (blue). Scale bar, 10 μm. ***c***, CASK association with Ch-SAP97-V decreases FRET efficiency. Ch-SAP97-V FRET efficiency was measured in HEK293 cells expressing the indicated Ch-SAP97-V and Myc-CASK constructs. When associated with CASK, Ch-SAP97-V FRET efficiency was decreased from 13.0 $\pm$ 1% to 2.2 $\pm$ 1.5% (mean $\pm$ SEM, $n = 20$ cells, $^*p < 0.001$). This decrease does not occur when CASKΔL27N is substituted for CASK (13.6 $\pm$ 0.7%; mean $\pm$ SEM, $n = 16$ cells). When the L27 domain L15K mutation was introduced to SAP97, only a partial decrease in L15K-Ch-SAP97-V FRET efficiency, from 12.7 $\pm$ 0.7% to 8.5 $\pm$ 0.6% (mean $\pm$ SEM, $n = 18$ cells), was observed when CASK was present. ***d***, L27 domain mutations disrupt the interaction between SAP97 and CASK. Wild-type and mutated SAP97 and CASK were coexpressed in HEK293 cells. Cell lysates were prepared, CASK-SAP97 complexes immunoprecipitated with anti-Myc antibody against the CASK tag and probed with anti-GFP (SAP97) and anti-Myc (CASK) antibodies. In the displayed representative Western blots, SAP97 only significantly coprecipitates with CASK when their respective L27 domains are intact. ***e***, CASK coexpression disrupts interactions between SAP97 and AMPARs. Cell lysates were prepared from HEK293 cells expressing Ch-GluA1 and GFP-SAP97 in the absence or presence of (*Figure legend continues.*)

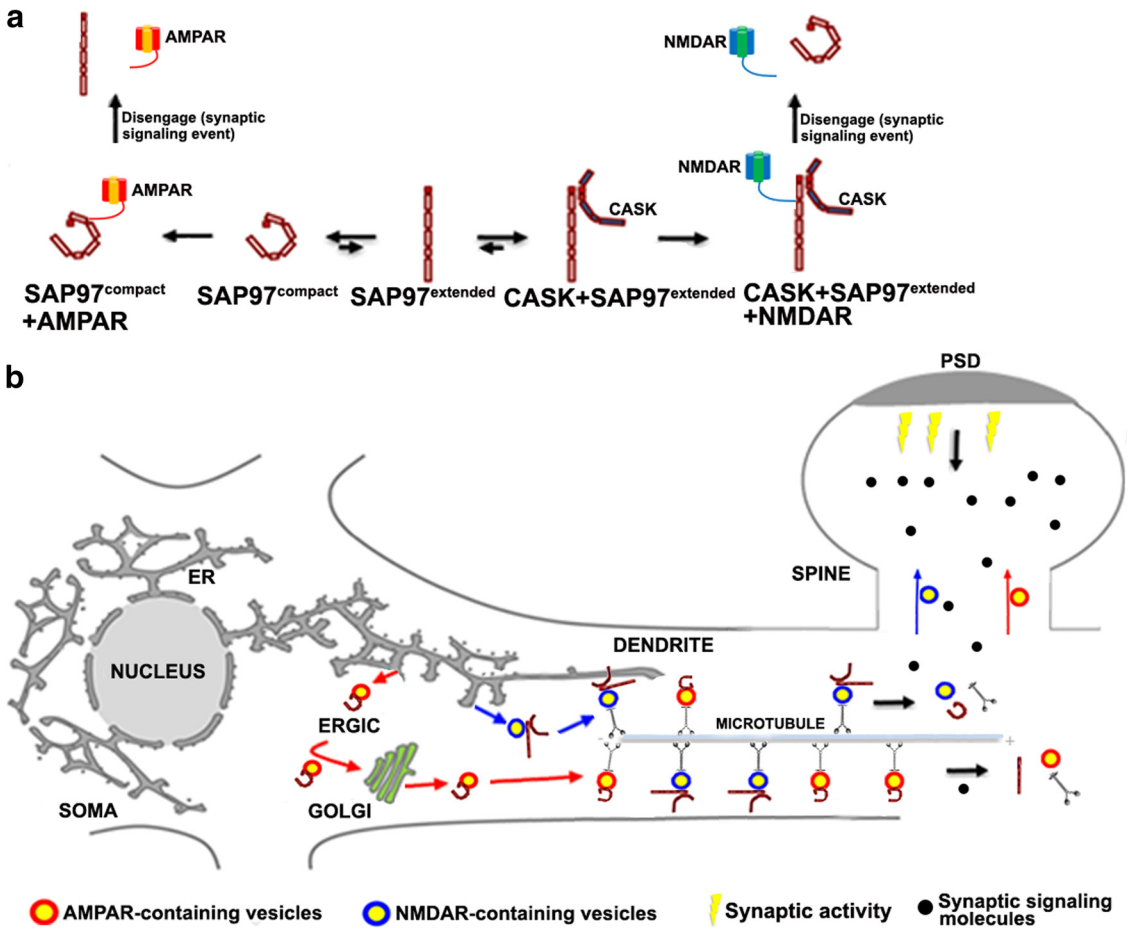

Figure 4. Model of SAP97 conformational changes, the role of CASK and the regulation of SAP97 interactions with AMPARs and NMDARs. ***a***, Proposed dynamic conformational changes of SAP97 *in vivo*. SAP97 is stabilized in the extended conformation when CASK binds to its L27 domain. The associations of the PDZ domains of SAP97 are changed by the transition from extended to compact conformation. In the compact conformation, SAP97 associates with the PDZ binding domain of the AMPAR subunit, GluA1, and in the extended conformation with the NMDAR subunit, GluN2B. CASK unbinding from SAP97 reverses the conformational change back to the compact conformation and causes the release of the GluN2B subunit. ***b***, Proposed role of SAP97 conformation in sorting, trafficking, and synaptic targeting of NMDARs and AMPARs.

complex of CASK and SAP97 bound to NMDARs in the ER recruits an additional set of binding partners that help mediate subsequent events. These events include the formation of ER-derived transport vesicles that contain ER-resident proteins as well as the CASK-SAP97-NMDAR complex (Jeyifous et al., 2009). In addition, CASK domains other than its L27N domain mediate interactions with a set of proteins that recruits an additional set of binding partners that link GluN2B-containing NMDARs to the kinesin motor, KIF17 (Setou et al., 2000). KIF17 moves NMDAR transport vesicles on microtubules in dendrites to a region near the synapse that the NMDARs will be trafficked to. When not bound by CASK, SAP97 is stabilized in the compact conformation that allows it to bind to AMPARs. Here it may play a parallel role in AMPAR trafficking and help recruit a different set of proteins linking it to another microtubule motor, such as KIF5 (Setou et al., 2000), which trafficks AMPARs in transport vesicles from the Golgi in the soma to their destinations in the dendrites.

Once NMDAR and AMPAR transport vesicles arrive at their destinations, they must disengage from microtubules in the shaft of the dendrite to allow the receptors to traffick to their specific postsynaptic membranes. We propose that a switch in SAP97 conformation could play an important role in synapse-specific targeting of NMDARs and AMPARs by causing the disengagement of cargo from microtubules and motors (Fig. 4). As shown in Figure 4, we assume that synaptic signaling events reverse SAP97 conformation, from extended to compact when bound to CASK and NMDARs, and from compact to extended when bound to AMPARs. The SAP97 conformation reversal, therefore, could result in NMDAR and AMPAR transport vesicle disengagement from their specific motors and microtubules. Subsequently, as shown in Figure 4*b*, NMDAR and AMPAR transport vesicles are free to engage myosin motors to traffick via the actin cytoskeleton into spines for synaptic targeting. The synaptic signaling events

←

(*Figure legend continued.*) Myc-CASK. Immunoprecipitations were performed with anti-GFP, specific for SAP97, and anti-RFP (GluA1) and anti-Myc (CASK) antibodies were used to probe membrane blots. Representative Western blots show a decrease in the amount of GluA1 that coprecipitates with SAP97 when CASK is coexpressed. Band intensities were normalized to values obtained in the absence of CASK coexpression. In the presence of CASK, coprecipitated GluA1 intensity decreased to 0.16 ± 0.02 (mean ± SEM, $n = 3$ independent experiments, $p < 0.001$). ***f***, Left graph, Peak FRET efficiency values for Ch-SAP97-V measured in HEK293 cells versus neurons. The values are as follows: 14.5 ± 1.0% (HEK293 cells), 25.9 ± 5.4% (neurons), and $^{*}p < 0.01$. Right graph, Peak FRET efficiency values for Ch-SAP97-V coexpressed with mutated CaMKII in HEK293 cells. Displayed are the mean peak FRET efficiency for Ch-SAP97-V alone, 12.5 ± 0.5%; Ch-SAP97-V + CaMKII-T286A, 9.6 ± 1.0%; Ch-SAP97-V + CaMKII-T286D, 16.6 ± 0.4%; $^{*}p < 0.01$, $^{**}p < 0.05$.

that specifically target NMDAR and AMPAR transport vesicles are unknown but may involve a "synaptic tagging" mechanism (Frey and Morris, 1998) and the synaptic activation of CaMKII (Lisman et al., 2012), which is trafficked into dendritic shafts at activated synaptic spines (Lemieux et al., 2012). Indeed, CaMKII phosphorylation of Mint1 correlates with the release of the NMDAR-containing transport vesicles from KIF17, a microtubule motor (Guillaud et al., 2008). CASK associates with Mint1 and is part of the adaptor complex linking NMDARs to KIF17 (Setou et al., 2000). CaMKII can alter SAP97 conformation (Fig. 3*f*), potentially altering its interaction with NMDARs. CaMKII phosphorylation of SAP97, which also complexes with CASK (Jeyifous et al., 2009), may augment the role of Mint1 in the release of transport vesicles by changing SAP97 from its extended to compact conformation and causing its release from NMDARs. CaMKII phosphorylation may also alter the interaction between SAP97 in the compact conformation and AMPARs in their transport vesicles by a similar mechanism.

An observation that appears to be at odds with the model is that SAP97 associates with NMDARs containing GluN2B when expressed without CASK in HEK293 cells (Fig. 2*b*; Jeyifous et al., 2009). This association could occur without CASK stabilizing SAP97 in the extended conformation via L27 domain-mediated multimerization of SAP97 (Nakagawa et al., 2004) triggering the change from compact to extended conformation, allowing it to bind to NMDARs. Alternatively, equilibrium between SAP97 states, although heavily favoring the compact state, could allow some SAP97 in a meta-stable extended state to interact with NMDARs in the absence of CASK (Fig. 4*a*). In the presence of NMDARs, which interact with extended SAP97, and in the absence of binding partners that stabilize SAP97 in the compact conformation, much of the SAP97 would end up interacting with NMDARs. In support of the latter explanation are our findings that CASK coprecipitates with SAP97 and GluN2B from brain lysates, colocalizes with NMDARs and SAP97 in cultured neurons, and CASK knockdown in cultured neurons has the same effect on NMDAR trafficking as SAP97 knockdown (Jeyifous et al., 2009). Also in support of this explanation is our finding that the distribution of SAP97 and GluN2B-containing NMDARs is very different when coexpressed with CASK. In the absence of CASK, SAP97 and NMDARs form large colocalized structures in the ER and fail to traffick to the cell surface. Addition of CASK prevents the formation of the structures and allows SAP97 and NMDARs to traffick to the cell surface, consistent with a significant change in the SAP97-NMDAR interaction (Jeyifous et al., 2009).

Our findings provide mechanistic insights into how SAP97 differentially engages and disengages with AMPARs and NMDARs at the ER and on separate transport vesicles. The structural basis of the changes in SAP97 conformation remains to be determined, as does whether similar conformational changes regulate other scaffolding proteins. We are currently focusing on how conformation is regulated by various post-translational modifications and how higher levels of regulation control these modifications. The alteration of SAP97 conformation by CaMKII (Fig. 3*f*) suggests that there are other mechanisms that regulate its conformation.

References

Bresler T, Shapira M, Boeckers T, Dresbach T, Futter M, Garner CC, Rosenblum K, Gundelfinger ED, Ziv NE (2004) Postsynaptic density assembly is fundamentally different from presynaptic active zone assembly. J Neurosci 24:1507–1520. CrossRef Medline

Claudio T (1992) Stable expression of heterologous multisubunit protein complexes established by calcium phosphate- or lipid-mediated cotransfection. Methods Enzymol 207:391–408. CrossRef Medline

Colledge M, Dean RA, Scott GK, Langeberg LK, Huganir RL, Scott JD (2000) Targeting of PKA to glutamate receptors through a MAGUK-AKAP complex. Neuron 27:107–119. CrossRef Medline

Elias GM, Nicoll RA (2007) Synaptic trafficking of glutamate receptors by MAGUK scaffolding proteins. Trends Cell Biol 17:343–352. CrossRef Medline

Feng W, Long JF, Fan JS, Suetake T, Zhang M (2004) The tetrameric L27 domain complex as an organization platform for supramolecular assemblies. Nat Struct Mol Biol 11:475–480. CrossRef Medline

Frey U, Morris RG (1998) Synaptic tagging: implications for late maintenance of hippocampal long-term potentiation. Trends Neurosci 21:181–188. CrossRef Medline

Gardoni F, Mauceri D, Fiorentini C, Bellone C, Missale C, Cattabeni F, Di Luca M (2003) CaMKII-dependent phosphorylation regulates SAP97/NR2A interaction. J Biol Chem 278:44745–44752. CrossRef Medline

Guillaud L, Wong R, Hirokawa N (2008) Disruption of KIF17-Mint1 interaction by CaMKII-dependent phosphorylation: a molecular model of kinesin-cargo release. Nat Cell Biol 10:19–29. CrossRef Medline

Ho SN, Hunt HD, Horton RM, Pullen JK, Pease LR (1989) Site-directed mutagenesis by overlap extension using the polymerase chain reaction. Gene 77:51–59. CrossRef Medline

Jeyifous O, Waites CL, Specht CG, Fujisawa S, Schubert M, Lin EI, Marshall J, Aoki C, de Silva T, Montgomery JM, Garner CC, Green WN (2009) SAP97 and CASK mediate sorting of NMDA receptors through a previously unknown secretory pathway. Nat Neurosci 12:1011–1019. CrossRef Medline

Karpova T, McNally JG (2006) Detecting protein-protein interactions with CFP-YFP FRET by acceptor photobleaching. Curr Protoc Cytom Chapter 12:Unit 12.7. CrossRef Medline

Kenworthy AK (2001) Imaging protein-protein interactions using fluorescence resonance energy transfer microscopy. Methods 24:289–296. CrossRef Medline

Lee S, Fan S, Makarova O, Straight S, Margolis B (2002) A novel and conserved protein-protein interaction domain of mammalian Lin-2/CASK binds and recruits SAP97 to the lateral surface of epithelia. Mol Cell Biol 22:1778–1791. CrossRef Medline

Lemieux M, Labrecque S, Tardif C, Labrie-Dion É, Lebel É, De Koninck P (2012) Translocation of CaMKII to dendritic microtubules supports the plasticity of local synapses. J Cell Biol 198:1055–1073. CrossRef Medline

Leonard AS, Davare MA, Horne MC, Garner CC, Hell JW (1998) SAP97 is associated with the alpha-amino-3-hydroxy-5-methylisoxazole-4-propionic acid receptor GluR1 subunit. J Biol Chem 273:19518–19524. CrossRef Medline

Lisman J, Yasuda R, Raghavachari S (2012) Mechanisms of CaMKII action in long-term potentiation. Nat Rev Neurosci 13:169–182. Medline

Mauceri D, Gardoni F, Marcello E, Di Luca M (2007) Dual role of CaMKII-dependent SAP97 phosphorylation in mediating trafficking and insertion of NMDA receptor subunit NR2A. J Neurochem 100:1032–1046. CrossRef Medline

McGee AW, Dakoji SR, Olsen O, Bredt DS, Lim WA, Prehoda KE (2001) Structure of the SH3-guanylate kinase module from PSD-95 suggests a mechanism for regulated assembly of MAGUK scaffolding proteins. Mol Cell 8:1291–1301. CrossRef Medline

Nakagawa T, Futai K, Lashuel HA, Lo I, Okamoto K, Walz T, Hayashi Y, Sheng M (2004) Quaternary structure, protein dynamics, and synaptic function of SAP97 controlled by L27 domain interactions. Neuron 44:453–467. CrossRef Medline

Nash JE, Appleby VJ, Corrêa SA, Wu H, Fitzjohn SM, Garner CC, Collingridge GL, Molnár E (2010) Disruption of the interaction between myosin VI and SAP97 is associated with a reduction in the number of AMPARs at hippocampal synapses. J Neurochem 112:677–690. CrossRef Medline

Perestenko PV, Henley JM (2003) Characterization of the intracellular transport of GluR1 and GluR2 alpha-amino-3-hydroxy-5-methyl-4-isoxazole propionic acid receptor subunits in hippocampal neurons. J Biol Chem 278:43525–43532. CrossRef Medline

Sans N, Racca C, Petralia RS, Wang YX, McCallum J, Wenthold RJ (2001) Synapse-associated protein 97 selectively associates with a subset of

AMPA receptors early in their biosynthetic pathway. J Neurosci 21:7506–7516. Medline

Setou M, Nakagawa T, Seog DH, Hirokawa N (2000) Kinesin superfamily motor protein KIF17 and mLin-10 in NMDA receptor-containing vesicle transport. Science 288:1796–1802. CrossRef Medline

Setou M, Seog DH, Tanaka Y, Kanai Y, Takei Y, Kawagishi M, Hirokawa N (2002) Glutamate-receptor-interacting protein GRIP1 directly steers kinesin to dendrites. Nature 417:83–87. CrossRef Medline

Tavares GA, Panepucci EH, Brunger AT (2001) Structural characterization of the intramolecular interaction between the SH3 and guanylate kinase domains of PSD-95. Mol Cell 8:1313–1325. CrossRef Medline

Tully MD, Grossmann JG, Phelan M, Pandelaneni S, Leyland M, Lian LY (2012) Conformational characterization of synapse-associated protein 97 by nuclear magnetic resonance and small-angle X-ray scattering shows compact and elongated forms. Biochemistry 51:899–908. CrossRef Medline

Waites CL, Specht CG, Härtel K, Leal-Ortiz S, Genoux D, Li D, Drisdel RC, Jeyifous O, Cheyne JE, Green WN, Montgomery JM, Garner CC (2009) Synaptic SAP97 isoforms regulate AMPA receptor dynamics and access to presynaptic glutamate. J Neurosci 29:4332–4345. CrossRef Medline

Washbourne P, Bennett JE, McAllister AK (2002) Rapid recruitment of NMDA receptor transport packets to nascent synapses. Nat Neurosci 5:751–759. Medline

Wu H, Reuver SM, Kuhlendahl S, Chung WJ, Garner CC (1998) Subcellular targeting and cytoskeletal attachment of SAP97 to the epithelial lateral membrane. J Cell Sci 111:2365–2376. Medline

Wu H, Reissner C, Kuhlendahl S, Coblentz B, Reuver S, Kindler S, Gundelfinger ED, Garner CC (2000) Intramolecular interactions regulate SAP97 binding to GKAP. EMBO J 19:5740–5751. CrossRef Medline

Xu W (2011) PSD-95-like membrane associated guanylate kinases (PSD-MAGUKs) and synaptic plasticity. Curr Opin Neurobiol 21:306–312. CrossRef Medline